

Helium isotope studies in the Mojave Desert, California: implications for groundwater chronology and regional seismicity

Justin T. Kulongoski^{a,*}, David R. Hilton^{a,2}, John A. Izbicki^{b,3}

^a*Fluids and Volatiles Laboratory, Scripps Institution of Oceanography, Geoscience Research Division,
University of California, San Diego, La Jolla, CA 92093-0244, USA*

^b*U.S. Geological Survey, Water Resources Division, San Diego, CA 92123, USA*

Received 23 December 2002; accepted 30 July 2003

Abstract

We report helium isotope and concentration results for groundwaters from the western Mojave River Basin (MRB), 130 km east of Los Angeles, CA. The basin lies adjacent to the NW–SE trending San Andreas Fault (SAF) system. Samples were collected along two groundwater flowpaths that originate in the San Gabriel Mountains and discharge to the Mojave River located ~ 32 km to the northeast. Additional groundwater samples were collected from Mojave River Deposits underlying the Mojave River. The primary objective of this study is to identify and quantify crustal and mantle helium contributions to the regional groundwater system.

A total of 27 groundwaters, sampled previously for chemistry and isotope systematics (including ¹⁴C activity) have measured helium concentrations that increase along flowpaths from 9.9×10^{-8} to 1.0×10^{-4} cm³ STP g⁻¹ H₂O. Concomitantly, ³He/⁴He ratios decrease from 0.84R_A to 0.11R_A (R_A equals the ³He/⁴He ratio in air = 1.4×10^{-6}). We did not record ³He/⁴He ratios equivalent to crustal-production values (~ 0.02R_A) in any sample.

Dissolved helium concentrations were resolved into components associated with solubility equilibration, air entrainment, mantle-derivation, in-situ production within the aquifer, and extraneous crustal fluxes. All samples contained the first four components, but only older samples had the superimposed effects of helium derived from a crustal flux. The radiogenic He component has chronological significance, and good concordance between ⁴He and ¹⁴C ages for younger groundwaters (<25,000 year) demonstrates the integrity of the ⁴He-chronometer in this setting. Helium-rich waters could also be dated with the ⁴He technique, but only by first isolating the whole crustal flux ($3-10 \times 10^{-6}$ cm³ STP cm⁻² year⁻¹). Mantle-derived ³He (³He_m) is present in all MRB samples irrespective of distance from the SAF. However, regional-aquifer groundwaters near the terminus of the flowpath have a significantly greater content of mantle-derived ³He in comparison with more modern samples. We propose that faults in the basin other than the SAF may be an additional source of mantle-derived helium. The large range in ³He_m concentrations may be related to fault activity; however, groundwaters with lower and more constant ³He_m contents may indicate that seismic activity along the SAF has been

* Corresponding author. Fax: +1-858-822-3310.

E-mail addresses: kulongos@usgs.gov, oski@ucsd.edu (J.T. Kulongoski), drhilton@ucsd.edu (D.R. Hilton), jaizbicki@usgs.gov (J.A. Izbicki).

¹ Now at U.S. Geological Survey, San Diego, CA 92123, USA.

² Fax: +1-858-822-3310.

³ Fax: +1-858-637-9201.

relatively constant for the past 30,000 years, demonstrating that ancient groundwaters may serve as an archive for paleo-seismic events.

© 2003 Elsevier B.V. All rights reserved.

Keywords: Helium isotope; Noble gas; Groundwater; Hydrology; Geochemistry

1. Introduction

The inert nature of the noble gases, coupled with their distinctive isotopic and solubility characteristics, makes them ideal tracers in groundwater-related studies. Their applicability extends across topics as diverse as groundwater dating, paleoclimatology, mechanism(s) of recharge, and mantle and seismic studies (see reviews by Ballentine et al., 2002; Kipfer et al., 2002). Helium has proven particularly useful owing to its low solubility in water, making it less susceptible to air contamination, large subsurface production rates (particularly of the ^4He isotope), and large and diagnostic variations in its isotopic composition ($^3\text{He}/^4\text{He}$ ratios), which impart critical information on fluid provenance and subsequent flow history. These attributes have led to the widespread exploitation of helium isotopes in groundwater-related studies, often independently of the other noble gases (e.g. Davis and DeWiest, 1966).

In this study, we present helium isotope and concentration results for groundwaters from the Mojave River Basin (MRB) in the high desert region of southern California. This groundwater system is well studied (e.g. Izbicki et al., 1995; Lines, 1996) owing to the pressing need to delineate groundwater resources in this area of rapid population growth. As such, the application of helium studies, particularly their ability to quantify groundwater chronologies, is a powerful addition to the array of techniques employed in the region aimed at quantifying flow history. Significantly, however, the MRB is also located immediately adjacent to the San Andreas Fault (SAF) system, imparting a tectonic component to the study. Prior work has shown that mantle-derived helium, identified by high $^3\text{He}/^4\text{He}$ ratios, is closely associated with fluid movement in and around the SAF system (Kennedy et al., 1997). In this study, therefore, we have the opportunity to combine

two distinct facets of helium isotope geochemistry, i.e. assessing the applicability of the He geochronometer in this area of recent tectonics as well as evaluating the magnitude and extent of mantle-derived volatile fluxing into the regional groundwater system. In this latter respect, an important aim of this study is to determine the viability of ancient groundwater as an archive for paleo-seismic events in the region.

2. Western Mojave River Basin, California

The Mojave River Basin (MRB) is located ~ 130 km northeast of Los Angeles in the Mojave Desert of southern California (Fig. 1). The basin occupies an area of 3626 km² and receives drainage from the San Gabriel and San Bernardino Mountains. It lies in a semi-arid region with low annual rainfall (< 150 mm year⁻¹), low humidity, and high summer temperatures. Infrequent transient storms cause intermittent flow in the Mojave River, which represents the only surface drainage of the area. In the high mountains, perennial surface flows emerge from outcropping bedrock.

Quaternary alluvium fills the basin, forming a gently sloping alluvial plain with three water-bearing units: younger (Qr) and ancestral (QTr) Mojave River Deposits, and undifferentiated alluvium (QTa) (see Fig. 2). The Mojave River Deposits (MRD) are composed of unconsolidated Pleistocene–Holocene fill that include a 60-m thick fluvial deposit base (QTr) underlying 20 m of younger river deposits (Qr). Groundwater in the MRD originates as lower altitude precipitation, and is recharged by infiltration of intermittent streamflow as well as directly from the Mojave River during floodflows (Izbicki, in preparation). Waters from the MRD contain low concentrations of dissolved solids, and are predominantly Na–HCO₃⁻ type.

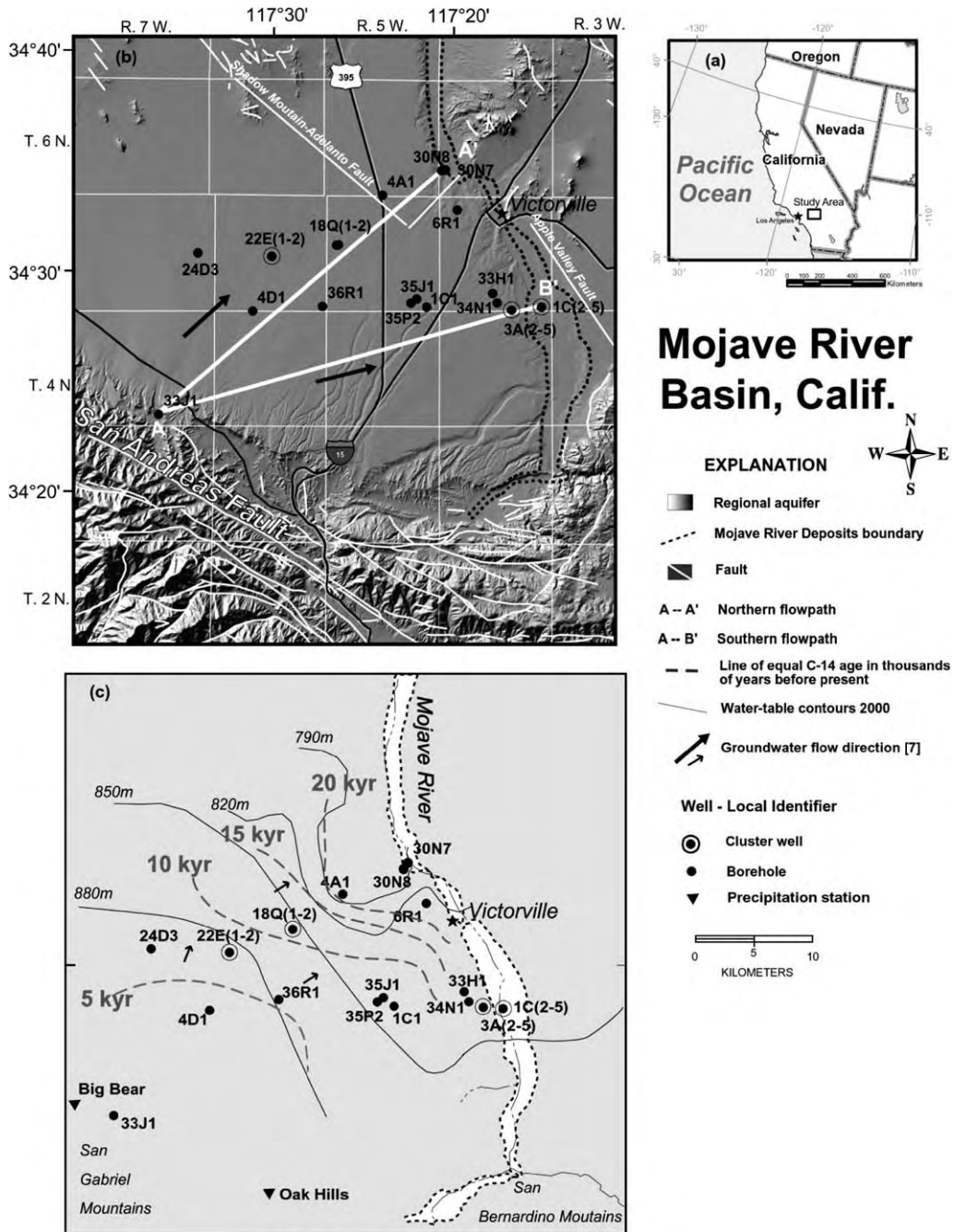


Fig. 1. (a) Regional map of southwestern USA showing study area. (b) Map of the Western Mojave River Basin (MRB) study area identifying the location of sampled boreholes (●). Direction of groundwater flow indicated with black arrows, flowpaths/geological cross-sections marked A–A', and A–B', and the regional fault system shown by white lines. (c) Hydrologic map of the MRB study area displaying age structure from carbon-14 (dashed gray lines) and peizometric surface contours (solid lines) projected along with borehole and precipitation-station locations. Groundwater flow direction indicated with black arrows.

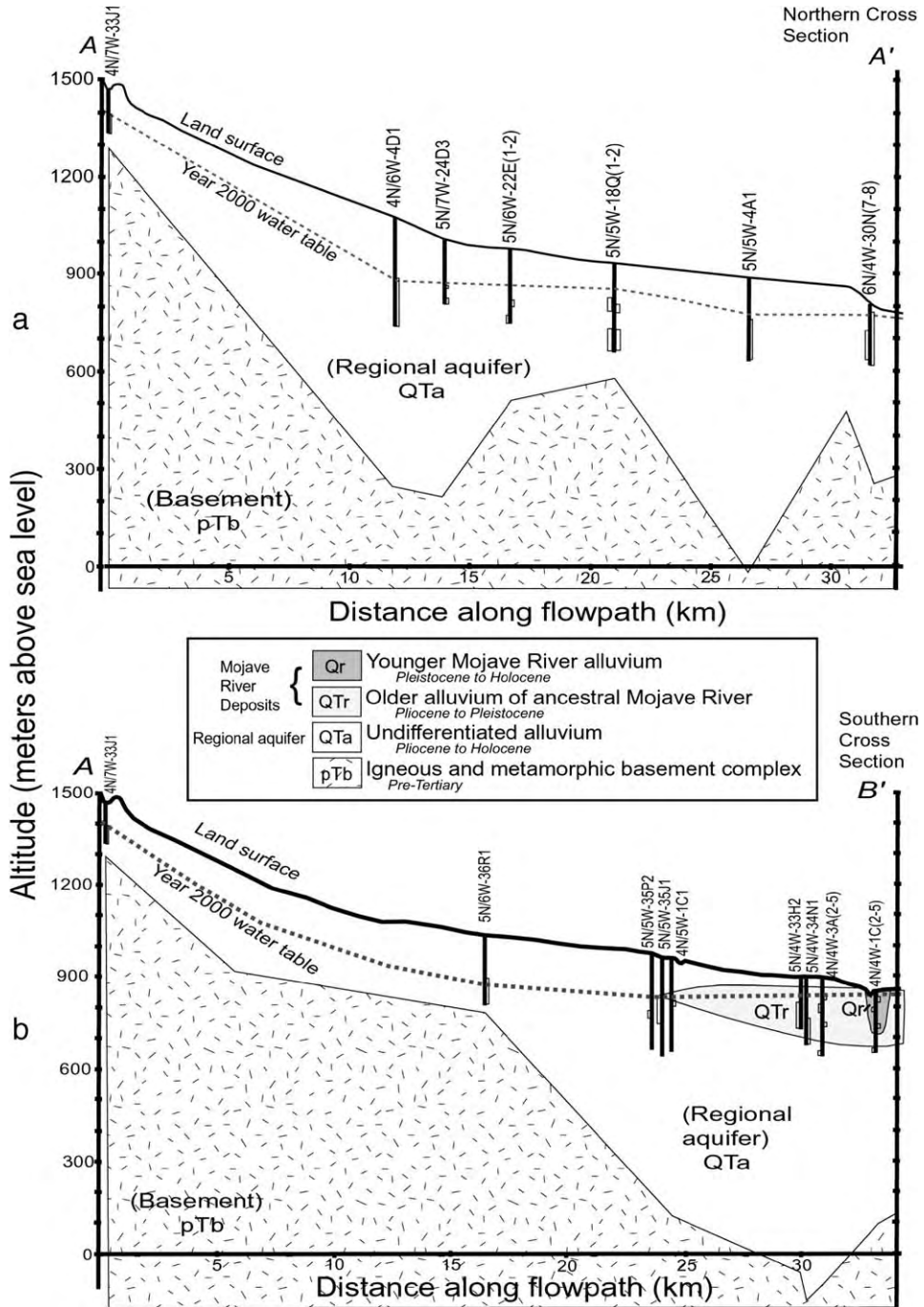


Fig. 2. Geological cross-sections of study area showing sampled boreholes and lithology from Fig. 1a, redrawn from (Stamos et al., 2001). (a) Cross-section of northern flow path A–A', (b) cross-section of southern flowpath A–B'. 2000 water table indicated by dashed line. Perforated section of bore hole casing indicated by open boxes. Vertical exaggeration 8:100.

The undifferentiated alluvium (QTa), which forms the regional aquifer, is more than 1000 m thick at some locations (Subsurface Surveys, 1990), and consists of alluvial and basin-fill deposits that are partly cemented and finer grained in comparison with the more permeable MRD (Fig. 2). These deposits (QTa) consist of unconsolidated to moderately consolidated gravel, sand, silt, and clay deposited in the Pleistocene and late Pliocene, and overlie a crystalline complex of igneous and metamorphic rocks (pTb), (California Dept. of Water Resources, 1967). Waters from this mostly unconfined aquifer contain, on average, higher concentrations of dissolved solids compared to the MRD; however, they are also predominantly Na–HCO₃⁻ type. Recharge to the regional aquifer occurs from the infiltration of higher altitude precipitation runoff through a 10–130 m thick unsaturated zone in the upper reaches of normally dry streambeds in the San Bernardino and San Gabriel Mountains. No recharge is currently observed away from the mountain front (Izbicki et al., 1998, 2000).

Within the MRB study area, there are three regional faults in addition to the SAF system. These faults are identified on the basis of (a) impedance to groundwater flow resulting in large drops in water levels, and (b) fault exposures within the river terraces (Stamos et al., 2001). The Shadow Mountain and Adelanto Faults (SMAF) act as partial barriers to slow groundwater flow along the northern flowpath (A–A'), and the NW–SE trending Apple Valley Fault (AVF) occurs just east of the Mojave River (Fig. 1).

A detailed picture has emerged of the hydrogeology of the MRB particularly regarding source, movement, and age structure of the groundwater (Izbicki et al., 1995, 1998; Stamos et al., 2001). In both aquifers, groundwater flow is toward the north–northeast (Fig. 1c). Whereas groundwater in the MRD is recharged intermittently as a result of stream leakage and from flood-flows in the Mojave River, the regional aquifer is recharged by infiltration of storm runoff in ephemeral stream channels (mountain-front recharge). Consequently, groundwater in the MRD has been recharged relatively recently, whereas the regional (deeper) aquifer contains a significant component of older waters, varying in age from ~150 year to >30,000 year (Izbicki et al., 1995; Izbicki and Michel, in preparation).

3. Hydrochemical background ($\delta^{18}\text{O}$, δD , ^3H , and ^{14}C)

Orographic effects control the stable isotope characteristics of groundwaters in the region. In turn, the stable isotopes provide a means of distinguishing groundwaters recharged by different mechanisms in different parts of the MRB (Fig. 3). Friedman et al. (1992) showed that the majority of precipitation events in the area occur as winter storms, originating over the central or northern Pacific Ocean before passing over high mountains to reach the Mojave Desert. Winter precipitation at Big Bear station, at an altitude of 2055 m in the San Gabriel Mountains, has mean δD and $\delta^{18}\text{O}$ values of -79‰ and -11.5‰ , respectively, and is the source of modern recharge to the regional aquifer (Friedman et al., 1992; Izbicki, in preparation). However, most groundwaters from the regional aquifer have δD and $\delta^{18}\text{O}$ values lighter than this value ($\delta\text{D} = -78.4\text{‰}$ to -96.4‰ with $\delta^{18}\text{O}$ values from -10.95‰ to -13.20‰), indicating that waters were recharged in climatic conditions considerably different from those of the present-day (Izbicki et al., 1995; Smith et al., 1992).

Precipitation collected at lower altitudes (the Cajon Pass at Oak Hills, altitude 1250 m; see Fig. 1c) has a distinct stable isotope signature owing to orographic effects (mean δD and $\delta^{18}\text{O}$ values of -63‰ and -9.1‰ , respectively; Friedman et al., 1992; Izbicki, in preparation). Groundwaters from the MRD (units Qr and QTr) have $\delta^{18}\text{O}$ and δD values close to those of lower altitude precipitation ($\delta^{18}\text{O} < -10.2\text{‰}$ and $\delta\text{D} < -71.6\text{‰}$, Fig. 3). This observation is consistent with higher ^3H and ^{14}C activities of waters in the MRD (Table 1) indicating recharge by more recent waters. The distinct stable isotope characteristics of the two aquifer systems, together with their different slopes in δD vs. $\delta^{18}\text{O}$ space (Fig. 3), reinforce the notion that the waters in the two aquifer systems were recharged at different times and under different prevailing conditions.

Carbon-14 data (together with corresponding $\delta^{13}\text{C}$ values) are available for the majority of the MRB groundwater samples included in this work. ^{14}C activities range from 95% to less than 0.5% modern carbon (Izbicki et al., 1995; Izbicki and Michel, in

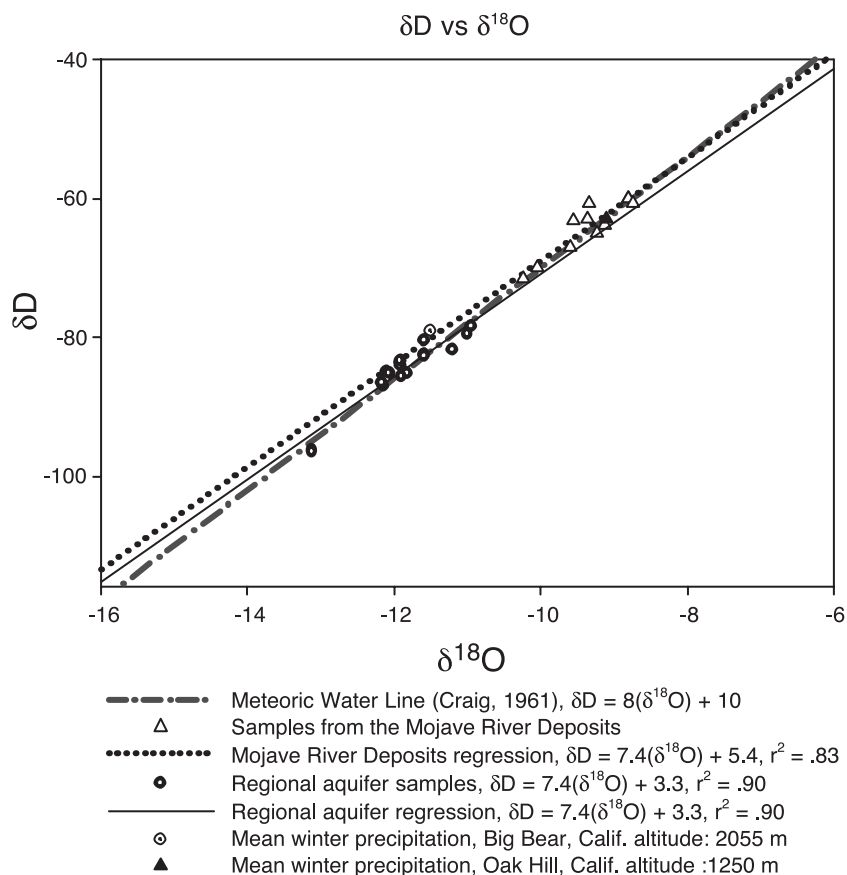


Fig. 3. δD vs. $\delta^{18}O$ for MRB groundwater samples plotted with respect to the Meteoric Water Line (dash-dot line). The two aquifers (regional and Mojave River Deposits) are distinguished by the stable isotope distributions with regression for the regional aquifer samples (solid black line), and regression for the Mojave River Deposits (dotted line). Open circle is the mean winter stable isotope values for precipitation at Big Bear station, altitude 2055 m. Black triangle is mean winter stable isotope value for precipitation at Oak Hill, altitude 1250 m.

preparation). Interpreted ^{14}C ages (in years), calculated using the program NETPATH (Plummer et al., 1994), are given in Table 1 (Izbicki et al., 1995). Typical uncertainties associated with interpreted ^{14}C groundwater ages are of the order of $\sim 20\%$, and are primarily controlled by knowledge of chemical interactions within the groundwater system (Davis and Bentley, 1982). The ages of MRD groundwaters are $< 10,000$ years, whereas the regional aquifer has some waters $> 30,000$ years, at the upper limit of the ^{14}C dating methodology. Along the northern flowpath ($A-A'$), ^{14}C water ages increase from ~ 150 years at site 4N/7W-33J1 near the mountain front, to $> 30,000$ years at site 6N/4W-30N8 near the

Mojave River. The southern flowpath ($A-B'$) shows a similar trend with ^{14}C groundwater ages increasing to $> 30,000$ years at site 4N/4W-1C2 also located near the Mojave River (Fig. 1b). The distance between the recharge zone and the discharge site 6N/4W-30N8 (32 km) divided by the ^{14}C age of the water (38,500 years) at that site gives an estimate of the groundwater flow velocity ($= 0.83 \text{ m year}^{-1}$). This value agrees with flow velocities determined using the MODFLOW groundwater model ($\sim 1 \text{ m year}^{-1}$) based on piezometric constraints (Stamos et al., 2001).

Shallow water in the MRD (e.g. 4N/4W-3A4) is significantly younger than the water in the underlying

Table 1

Helium and neon data for the Mojave River Basin (including ^{14}C and ^3H , see footnotes for details)

MRB township/range borehole ID	Distance (km)	$^{14}\text{C}^{\text{a}}$ (years) ($\pm 20\%$)	$^3\text{H}^{\text{b}}$ (TU)	$^4\text{He}_{\text{s}}$ ($\times 10^{-7}$) ($\text{cm}^3 \text{STP g}^{-1}$)	$R_{\text{s}}/R_{\text{A}}^{\text{c}}$	Ne_{s} ($\pm 1\%$) ($\times 10^{-7}$)	Ne_{a} ($\pm 2\%$) ($\text{cm}^3 \text{STP g}^{-1}$)	$^4\text{He}_{\text{a}}$ ($\pm 10\%$)	$^4\text{He}_{\text{ex}}$ ($\pm 7\%$)	$(R_{\text{ex}}/R_{\text{A}})$ ($\pm 7\%$)	He age (years)
<i>Regional aquifer—Northern flowpath (A–A')</i>											
4N/7W-33J1	0.5	150	nd	1.18 ± 0.02	0.84 ± 0.02	3.07	1.09	0.31	0.38	0.55	1250 ^d
4N/6W-4D1	11.9	5580	nd	1.62 ± 0.02	0.75 ± 0.04	3.91	1.93	0.56	0.58	0.33	6980 ^d
replicate	11.9	5580	nd	4.03 ± 0.06	0.84 ± 0.03	10.96	8.98	2.59	0.94	0.37	11,300 ^d
5N/7W-24D3	14.1	19,990	nd	1.58 ± 0.02	0.77 ± 0.03	3.99	2.01	0.58	0.52	0.35	6660 ^d
5N/6W-22E1	16.5	41,350	nd	4.08 ± 0.06	0.40 ± 0.02	4.92	2.94	0.85	2.74	0.12	23,300 ^d
5N/6W-22E2	16.5	23,280	nd	1.80 ± 0.03	0.78 ± 0.04	4.56	2.58	0.74	0.57	0.34	5370 ^d
5N/5W-18Q1	20.91	11,880	0.01	2.01 ± 0.03	0.62 ± 0.03	3.83	1.85	0.53	1.00	0.25	7020 ^d
5N/5W-18Q2	20.94	nd	nd	3.33 ± 0.05	0.79 ± 0.02	6.74	4.76	1.37	1.41	0.55	9600 ^d
5N/5W-4A1 ^e	26.5	28,500	nd	290 ± 4	0.121 ± 0.002	3.79	1.81	0.52	285	0.12	20,600 ^f
6N/4W-30N8 ^e	31.8	38,500	nd	1015 ± 15	0.116 ± 0.002	4.03	2.05	0.59	1001	0.11	44,000 ^f
<i>Regional aquifer—Southern flowpath (A–B')</i>											
4N/7W-33J1	0.5	150	nd	1.18 ± 0.02	0.84 ± 0.02	3.07	1.09	0.31	0.38	0.55	1250 ^d
5N/6W-36R1	16.5	nd	nd	3.26 ± 0.05	0.42 ± 0.02	4.36	2.38	0.69	2.09	0.11	3210 ^d
5N/5W-35P2	23.5	nd	nd	3.86 ± 0.06	0.40 ± 0.05	4.74	2.76	0.79	2.57	0.11	14,200 ^g
5N/5W-35J1	24.1	nd	nd	4.16 ± 0.06	0.52 ± 0.02	6.37	4.39	1.27	2.38	0.19	13,600 ^g
4N/5W-1C1	24.6	12,300	nd	4.14 ± 0.06	0.31 ± 0.01	3.22	1.24	0.36	3.27	0.14	19,300 ^g
4N/4W-3A2 ^e	31.3	26,320	0.05	134 ± 2	0.116 ± 0.002	4.11	2.13	0.61	131	0.11	32,500 ^h
4N/4W-1C2 ^e	33.9	37,500	0.09	187 ± 3	0.119 ± 0.002	3.54	1.56	0.45	184	0.11	34,500 ^h
<i>Mojave River deposits</i>											
4N/4W-3A5	14.3	nd	0.05	0.99 ± 0.02	0.94 ± 0.05	3.36	1.48	0.43	0.11	0.55	30 ^h
4N/4W-3A4	14.3	112	0.05	1.55 ± 0.02	1.00 ± 0.04	5.60	3.72	1.07	0.02	1.26	10 ^h
4N/4W-3A3	14.3	5000	0.05	3.52 ± 0.05	0.48 ± 0.01	4.89	3.00	0.85	1.76	0.18	590 ^h
Replicate	14.3	5000	0.05	3.11 ± 0.04	0.52 ± 0.02	4.88	3.01	0.87	2.16	0.17	480 ^h
4N/4W-1C5	14.4	nd	5.1	1.36 ± 0.02	0.89 ± 0.06	4.97	3.09	0.89	0.03	-7.94	10 ^h
4N/4W-1C4	14.4	nd	12.2	1.47 ± 0.02	1.24 ± 0.06	5.21	3.33	0.96	0.01	7.2	0 ^h
4N/4W-1C3	14.4	1215	0.12	3.15 ± 0.05	0.53 ± 0.02	5.07	3.19	0.92	1.75	0.16	380 ^h
5N/4W-34N1	14.5	1500	nd	14.8 ± 0.2	0.216 ± 0.007	5.08	3.20	0.92	13.2	0.14	4050 ^h
5N/4W-33H2	14.6	nd	nd	1.43 ± 0.02	0.88 ± 0.02	4.74	2.85	0.82	0.16	0.01	50 ^h
5N/4W-6R1	25.0	8000	nd	8.3 ± 0.1	0.243 ± 0.007	4.26	2.38	0.69	7.06	0.12	750 ^h
6N/4W-30N7 ^e	28.1	4477	0.32	212 ± 3	0.113 ± 0.002	3.63	1.75	0.50	208	0.11	8750 ^f

nd—No data available.

He and Ne concentrations ($\times 10^{-7}$) in $\text{cm}^3 \text{STP g}^{-1}$.Regional aquifer $\text{He}_{\text{eq}} = 4.61 \times 10^{-8}$ in $\text{cm}^3 \text{STP g}^{-1}$; Mojave River Deposits $\text{He}_{\text{eq}} = 4.50 \times 10^{-8}$ in $\text{cm}^3 \text{STP g}^{-1}$.

4N/7W-33J1 is the origin of both flowpaths.

^a Interpreted ^{14}C ages from (Izbicki and Michel, in preparation).^b ^3H values from (Izbicki and Michel, in preparation).^c Helium ratio in air, $R_{\text{A}} = 1.4 \times 10^{-6}$.^d Helium ages calculated with $\phi = 0.2$ and $J_0 = 3 \times 10^{-8}$.^e Terminal site (>22 km along flowpath).^f Helium ages calculated with $\phi = 0.1$ and $J_0 = 1 \times 10^{-5}$.^g Helium ages calculated with $\phi = 0.1$ and $J_0 = 3 \times 10^{-8}$.^h Helium ages calculated with $\phi = 0.1$ and $J_0 = 3 \times 10^{-6}$.

regional aquifer (e.g. 4N/4W-3A2) because surface flows along the entire length of the Mojave River infiltrate the shallow aquifer system. As a result, the

age of the groundwater in the MRD does not increase along the flowpaths as it does in the regional aquifer system.

4. Analytical methods

Of the 25 boreholes sampled for this study (21 in May 2000 and 4 in June 2001), 15 are 24-cm ID production wells equipped with electric turbine pumps, and 10 are 6-cm ID multi-level observation wells (4N/4W-3A(2–5), 4N/4W-1C(2–5), 5N/6W-22E(1–2)) sampled using a Bennet submersible pump. The multi-level wells represent spatially restricted arrays of wells that penetrate to different depths in the aquifer. In this way, multi-level wells 4N/4W-3A(2–5) and 4N/4W-1C(2–5) sample both the MRD and the underlying regional aquifer (see Fig. 2).

A total of 15 groundwaters from the regional aquifer and 10 from the MRD were sampled. The regional aquifer samples follow two groundwater flowpaths (a northern path $A-A'$ and a southern path $A-B'$; Fig. 1) that extend from the foothills of the San Gabriel Mountains down the alluvial slope to the Mojave River. These flowpaths have been delineated by field measurements, groundwater chemistry, isotopic studies, and regional groundwater flow models (Izbicki et al., 1995; Stamos et al., 2001).

Prior to sampling, all boreholes were pumped to purge the equivalent of three volumes of the borehole casing in order to clear the wells of possible air-contaminated water. Pump outflow was then diverted through clear tubing connected to prepared annealed copper tubes. Following flushing, the copper tube was crimped with a Teamco® cold-welder, capturing a $\sim 14 \text{ cm}^3$ aliquot of groundwater in the sealed copper tube. The clear tubing allows the water samples to be visually inspected for air bubbles, prior to crimping. Collecting fluid samples in copper tubing allows sample storage for long periods without risk of compromising gas integrity.

Samples were analyzed for helium (isotopes and abundances) and neon (abundances) at the Fluids and Volatiles Laboratory of the Scripps Institution of Oceanography. Waters were released from the Cu-tubes under ultra high vacuum allowing ex-solution of dissolved gases (see Kulongoski and Hilton, 2002). This procedure was followed by isolation of the (He+Ne) fraction by a combination of gettering of the active gas fraction (using titanium-sponge held at $\sim 700 \text{ }^\circ\text{C}$) and sorption of the heavy noble gas fraction on activated charcoal ($-196 \text{ }^\circ\text{C}$). A known split ($\sim 0.4\%$) of the (He+Ne) fraction was then

expanded into a glass break seal and transferred to a magnetic sector mass spectrometer (MAP 215) and interfacing gas handling system. The He + Ne split was then further purified by exposure to a titanium sponge finger ($700 \text{ }^\circ\text{C}$) and charcoal finger ($-196 \text{ }^\circ\text{C}$) prior to exposure to a cryogenic trap designed to separate He from Ne. Helium and neon were inlet to the mass spectrometer sequentially. Sample peak intensities were compared with prepared standards of atmospheric air. Errors on $^3\text{He}/^4\text{He}$ ratios principally reflect counting statistics on the ^3He ion beam ($\pm < 4\%$), whereas errors on He and Ne contents also incorporate uncertainties associated with reproducibility of duplicate analyses (usually good to $\pm 2\%$).

5. Results

In Table 1, we report helium isotope and abundance results for 27 samples (including two replicate analyses) from the MRB. Results are reported as sample ^4He and Ne concentrations ($^4\text{He}_s$ and Ne_s) and sample $^3\text{He}/^4\text{He}$ ratios (reported as R_s/R_A , where R_s = sample $^3\text{He}/^4\text{He}$, and R_A is the air $^3\text{He}/^4\text{He}$ ratio = 1.4×10^{-6}). Note that sample 4N/7W-33J1 forms part of flowpath $A-A'$ and $A-B'$. Also included in Table 1 are borehole details including interpreted ^{14}C ages and tritium contents of the groundwaters (see table footnote for details).

5.1. Helium concentrations

Groundwater samples from the regional aquifer have measured helium concentrations (He_s) that increase from 1.18×10^{-7} to $1015 \times 10^{-7} \text{ cm}^3 \text{ STP g}^{-1} \text{ H}_2\text{O}$ along the northern flowpath ($A-A'$) and from 1.18×10^{-7} to $187 \times 10^{-7} \text{ cm}^3 \text{ STP g}^{-1} \text{ H}_2\text{O}$ along the southern flowpath ($A-B'$)—see Table 1. In all cases, He concentrations are in excess of air-equilibrated waters ($0.461 \times 10^{-7} \text{ cm}^3 \text{ STP g}^{-1} \text{ H}_2\text{O}$ —at $12 \text{ }^\circ\text{C}$), consistent with addition of extraneous He. Similarly, waters from the MRD also have He contents in excess of air-equilibrated values (range = 0.99×10^{-7} to $212 \times 10^{-7} \text{ cm}^3 \text{ STP g}^{-1} \text{ H}_2\text{O}$). Helium concentrations are also observed to increase with depth at the three multi-level observation wells: from 0.99×10^{-7} to $134 \times 10^{-7} \text{ cm}^3 \text{ STP g}^{-1} \text{ H}_2\text{O}$ at site 4N/4W-3A(2–5); from 1.36×10^{-7} to $187 \times 10^{-7} \text{ cm}^3 \text{ STP g}^{-1}$

H₂O at site 4N/4W-1C(2–5); and from 1.80×10^{-7} to 4.08×10^{-7} cm³ STPg⁻¹ H₂O at site 5N/6W-22E(1–2), (see Fig. 2 for perforation intervals in the multilevel wells).

5.2. Helium isotope ratios

Measured ³He/⁴He ratios (R_s/R_A) in the regional aquifer decrease from $0.84R_A$ to $0.12R_A$ along the northern flowpath and from $0.84R_A$ to $0.12R_A$ along the southern flowpath (Fig. 4 shows R_s/R_A values corrected for air bubble entrainment). Measured ³He/⁴He ratios are similarly low in the MRD ($0.11R_A$), but the highest value (borehole 4N/4W-

1C3 = $1.24R_A$) exceeds the ratio in air. This borehole has measurable tritium in the water (12.2 TU), indicating that the high ³He/⁴He value may be due in part to tritogenic ³He (see below and following section).

The lowest ³He/⁴He ratio measured in the MRB is $\sim 0.11R_A$, significantly greater than the helium isotope ratio anticipated for in-situ (radiogenic) production ($\sim 0.02R_A$) in typical crustal lithologies (Andrews, 1985; Ballentine and Burnard, 2002). The higher than expected ³He/⁴He ratios in the MRB samples could be explained as a result of several processes including in situ produced ³He and/or the preferential release of nucleogenic ³He, decay of tritiated water, or an influx of mantle ³He. Distin-

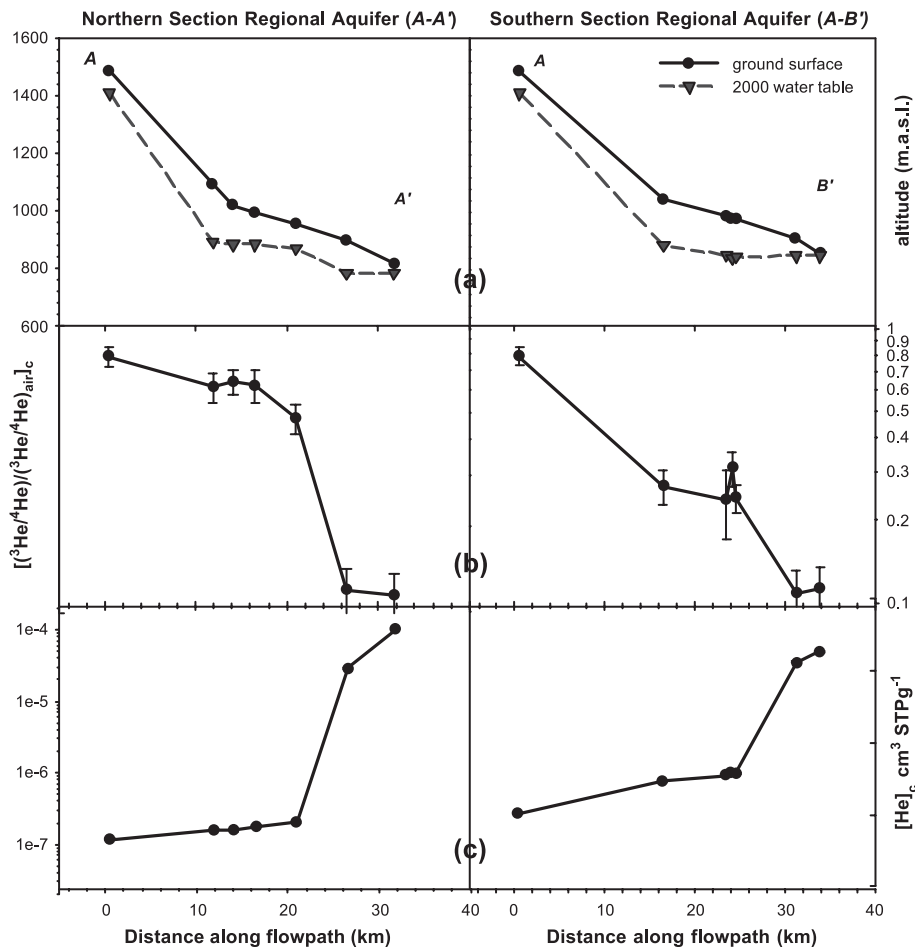


Fig. 4. (a) Land surface and 2000 water-table altitude, (b) evolution of ³He/⁴He compared to the ratio of air (R_s/R_A), corrected for air-bubble entrainment, and (c) helium concentrations (corrected for air-bubble entrainment), as a function of the distance from recharge in the San Gabriel Mountains along the cross-sections A–A' and A–B'.

guishing between these possibilities is covered in the following section.

6. Discussion

6.1. Resolution of helium components

Measured sample concentrations ($^3\text{He}_s$ and $^4\text{He}_s$) represent the sum of several helium components, which, upon resolution can provide insight into the provenance of helium fluxes into the groundwater system. These sources of helium (^3He and ^4He) include in situ production (He_{is}) from the decay of Li, U and Th in the aquifer matrix, a mantle flux (He_m), a deep crustal flux (He_{dc}), air-equilibrated helium (He_{eq}), dissolved-air bubbles (He_a), and tritogenic helium-3 ($^3\text{He}_t$). The helium-balance equation describing helium dissolved in groundwater (Stute et al., 1992; Torgersen, 1980) resolves the measured ratio of the sample (R_s) into its components:

$$R_s = \frac{^3\text{He}_s}{^4\text{He}_s} = \frac{^3\text{He}_{eq} + ^3\text{He}_a + ^3\text{He}_{is} + ^3\text{He}_{dc} + ^3\text{He}_m + ^3\text{He}_t}{^4\text{He}_{eq} + ^4\text{He}_a + ^4\text{He}_{is} + ^4\text{He}_{dc} + ^4\text{He}_m} \quad (1)$$

where $^3\text{He}_s$ and $^4\text{He}_s$ are the helium-3 and helium-4 concentrations measured in a groundwater sample.

Different sources of helium have distinct $^3\text{He}/^4\text{He}$ ratios, which are useful in distinguishing the various contributions to the measured value. Endmember $^3\text{He}/^4\text{He}$ ratios include mantle $R_m = 1.1 \times 10^{-5} = 8R_A$ (Craig and Lupton, 1981), and in situ and deep crustal $R_{is} \sim R_{dc} \sim 2 \times 10^{-8} = 0.02R_A$ sources (Mamyrin and Tolstikhin, 1984). For groundwaters >50 years, there is no nuclear bomb-derived ^3He , allowing the $^3\text{He}_t$ value to be assigned a background value ~ 2 TU (Michel, 1989).

6.1.1. Atmospheric components

The contribution of the atmospheric helium components, He_{eq} and He_a , to the total (measured) helium in the groundwater samples may be calculated using measured concentrations of helium, neon, the He/Ne ratio, and an adopted air-equilibration temperature (of

recharge) (Torgersen, 1980). Given the relative insensitivity of the solubility of He and Ne to temperature (Ozima and Podosek, 1983), the recharge temperature has a small effect on the concentrations of He and Ne, and can therefore be estimated from regional climate and groundwater temperature measurements. In this study, the temperature of recently recharged groundwater at the mountain-front was measured at 12 °C, while stream-flow temperature in the Mojave River was estimated to be 18 °C based on precipitation data along the Mojave River.

Calculation of the amounts of air-entrained He relies on the assumption that the dissolved neon measured in a sample can be represented solely as the sum of the neon from air-equilibration and air bubble entrapment:

$$\text{Ne}_s = \text{Ne}_{eq} + \text{Ne}_a \quad (2)$$

In Eq. (2) Ne_{eq} is known from the (estimated) equilibrium temperature and Ne_s is the measured neon concentration, which enables the calculation of Ne_a (see Table 1).

The amount of helium from entrained air bubbles, He_a , is then calculated using the helium–neon ratio in air ($\text{He}_a/\text{Ne}_a = 0.29$ (Weiss, 1971):

$$\text{He}_a = \left(\frac{\text{He}_a}{\text{Ne}_a} \times \text{Ne}_a \right) \quad (3)$$

In Table 1 we list the amounts of air-bubble-derived He and Ne for all samples from the MRB. Interestingly, samples collected from the Mojave River deposits contain higher amounts of entrained air (mean $\text{He}_a = 0.81 \times 10^{-7} \text{ cm}^3 \text{ STP g}^{-1} \text{ H}_2\text{O}$, $n=10$) than the northern (mean $\text{He}_a = 0.67 \times 10^{-7} \text{ cm}^3 \text{ STP g}^{-1} \text{ H}_2\text{O}$; $n=9$) or southern (mean $\text{Ne}_a = 0.64 \times 10^{-7} \text{ cm}^3 \text{ STP g}^{-1} \text{ H}_2\text{O}$; $n=7$) flowpaths of the regional aquifer. This may reflect large fluctuations in the water table during flood events of the Mojave River (e.g. rise of 26 m in 1993; Lines, 1996) resulting in dissolution of trapped air bubbles by excess water pressure (Kipfer et al., 2002). Further consideration of this topic is left to a companion work (Kulongoski et al., in preparation).

6.1.2. Terrigenous components

Helium in groundwater not of atmospheric origin is referred to as terrigenous or excess helium (He_{ex}), and

is the sum of in situ-produced, deep crustal and mantle-derived helium components. Excess helium-3 (${}^3\text{He}_{\text{ex}}$) is calculated using ${}^4\text{He}$ concentrations and the ${}^3\text{He}/{}^4\text{He}$ ratios assumed for the different sources (see Section 6.1):

$${}^3\text{He}_{\text{ex}} = ({}^4\text{He}_s \times R_s) - ({}^4\text{He}_{\text{eq}} \times R_{\text{eq}}) - ({}^4\text{He}_a \times R_a) \quad (4)$$

Excess helium-4 (${}^4\text{He}_{\text{ex}}$) is calculated by:

$${}^4\text{He}_{\text{ex}} = {}^4\text{He}_s - {}^4\text{He}_{\text{eq}} - {}^4\text{He}_a \quad (5)$$

From Eqs. (4) and (5), R_{ex} is the ${}^3\text{He}_{\text{ex}}/{}^4\text{He}_{\text{ex}}$ ratio.

The total helium of a sample may be separated into its various components by transforming the helium-balance equation Eq. (1), as described by Torgersen (1980) and Stute et al. (1992), into:

$$\begin{aligned} \frac{{}^3\text{He}_s - {}^3\text{He}_a}{{}^4\text{He}_s - {}^4\text{He}_a} &= \frac{{}^3\text{He}_{\text{eq}} + {}^3\text{He}_{\text{is}} + {}^3\text{He}_{\text{dc}} + {}^3\text{He}_{\text{m}} + {}^3\text{He}_{\text{t}}}{{}^4\text{He}_{\text{eq}} + {}^4\text{He}_{\text{is}} + {}^4\text{He}_{\text{dc}} + {}^4\text{He}_{\text{m}}} \quad (6) \\ &= \frac{({}^4\text{He}_{\text{eq}} \times R_{\text{eq}}) + ({}^4\text{He}_{\text{is}} \times R_{\text{is}}) + ({}^4\text{He}_{\text{dc}} \times R_{\text{dc}}) + ({}^4\text{He}_{\text{m}} \times R_{\text{m}}) + {}^3\text{He}_{\text{t}}}{{}^4\text{He}_s - {}^4\text{He}_a} \quad (7) \end{aligned}$$

R_{ex} is then defined from Eqs. (4) and (5) as:

$$R_{\text{ex}} = \frac{({}^4\text{He}_{\text{is}} \times R_{\text{is}}) + ({}^4\text{He}_{\text{dc}} \times R_{\text{dc}}) + ({}^4\text{He}_{\text{m}} \times R_{\text{m}})}{{}^4\text{He}_{\text{is}} + {}^4\text{He}_{\text{dc}} + {}^4\text{He}_{\text{m}}} \quad (8)$$

$$= \frac{({}^4\text{He}_{\text{is}} \times R_{\text{is}}) + ({}^4\text{He}_{\text{dc}} \times R_{\text{dc}}) + ({}^4\text{He}_{\text{m}} \times R_{\text{m}})}{{}^4\text{He}_{\text{ex}}} \quad (9)$$

Substituting (9) into Eq. (7) gives the linear equation ($Y = mX + b$) (Castro et al., 2000; Stute et al., 1992; Weise and Moser, 1987)

$$\begin{aligned} \frac{{}^3\text{He}_s - {}^3\text{He}_a}{{}^4\text{He}_s - {}^4\text{He}_a} &= \left(R_{\text{eq}} - R_{\text{ex}} + \frac{{}^3\text{He}_{\text{t}}}{{}^4\text{He}_{\text{eq}}} \right) \\ &\times \frac{{}^4\text{He}_{\text{eq}}}{{}^4\text{He}_s - {}^4\text{He}_a} + R_{\text{ex}} \quad (10) \end{aligned}$$

in which Y is the measured ${}^3\text{He}/{}^4\text{He}$ ratio corrected for air bubble entrainment, X is the fraction of ${}^4\text{He}$ in water resulting from air-equilibration with respect to

the total ${}^4\text{He}$ corrected for air bubble entrainment, and R_{ex} is the ${}^3\text{He}/{}^4\text{He}$ ratio of the excess (crustal and mantle) helium.

In Fig. 5, we plot Y versus X (as defined above) for MRB data to estimate (i) R_{ex} (the Y -axis intercept) which is the effective contribution of terrigenous helium to this system (including deep crustal and mantle fluxes), and (ii) the possible contribution of tritogenic ${}^3\text{He}$ (from the gradient) which is diagnostic of recent (young) water. In effect, this plot represents the evolution of the MRB groundwater system from recharge conditions (R_{eq}) in which all of the dissolved helium is from air-equilibration ${}^4\text{He}_{\text{eq}}/({}^4\text{He}_s - {}^4\text{He}_a) \sim 1$, to X -axis values dominated by crustal and/or mantle contributions, ${}^4\text{He}_{\text{eq}}/({}^4\text{He}_s - {}^4\text{He}_a) < 0.005$. Also included in Fig. 5 are trajectories representing the evolution of groundwater helium ratios from (i) the addition of radiogenic He with a ${}^3\text{He}/{}^4\text{He}$ ratio typical of crustal lithologies ($0.02R_A$, Ozima and Podosek, 1983)—line (a); (ii) addition of radiogenic He with a slightly higher ${}^3\text{He}/{}^4\text{He}$ ratio ($0.11R_A$ —equal to the lowest measured value)—line (b); (iii) addition of $0.5 \times 10^{-14} \text{ cm}^3\text{STP } {}^3\text{He}$ (representing complete decay of 2 TU) to evolutionary trajectory (b)—line (c); (iv) addition of $5.5 \times 10^{-14} \text{ cm}^3\text{STP } {}^3\text{He}$ (representing complete decay of 22 TU) to evolutionary trajectory (b)—line (d); and (v) for reference, the integrated effects of complete decay of 2 TU and a 10% addition of mantle helium ($8R_A$) to radiogenic He ($0.02R_A$)—line (e).

In Fig. 5, 19 of the 25 MRB samples plot (within error) between lines (b) and (c) which represent the respective evolution of the ${}^3\text{He}/{}^4\text{He}$ ratios from R_{eq} , and R_{eq} plus 2 TU, toward the helium excess ratio R_{ex} ($= 1.59 \times 10^{-7}$ or $0.11 R_A$). Also shown in Fig. 5 is a close-up plot of the Y -axis, focusing on the oldest, and therefore most evolved, groundwater samples (${}^4\text{He}_{\text{eq}}/({}^4\text{He}_s - {}^4\text{He}_a) < 0.005$). Included are lines (a, b, c, and d) as described above. This figure shows the five most evolved regional aquifer samples (closest the Y -axis)—the mean value of which ($1.59 \times 10^{-7} \pm 6\%$ at the 2σ level) is taken as the MRB R_{ex} value. We interpret this R_{ex} value as representative of the regional flux to the MRB groundwater system. It is noteworthy that this value is ~ 4 to 5 times higher than the expected deep crustal excess ratio R_{dc} ($= 0.02R_A$).

There are three possibilities that can explain the high value of R_{ex} : (i) mixing of older groundwater with younger post-bomb tritiated water, (ii) a contribution of

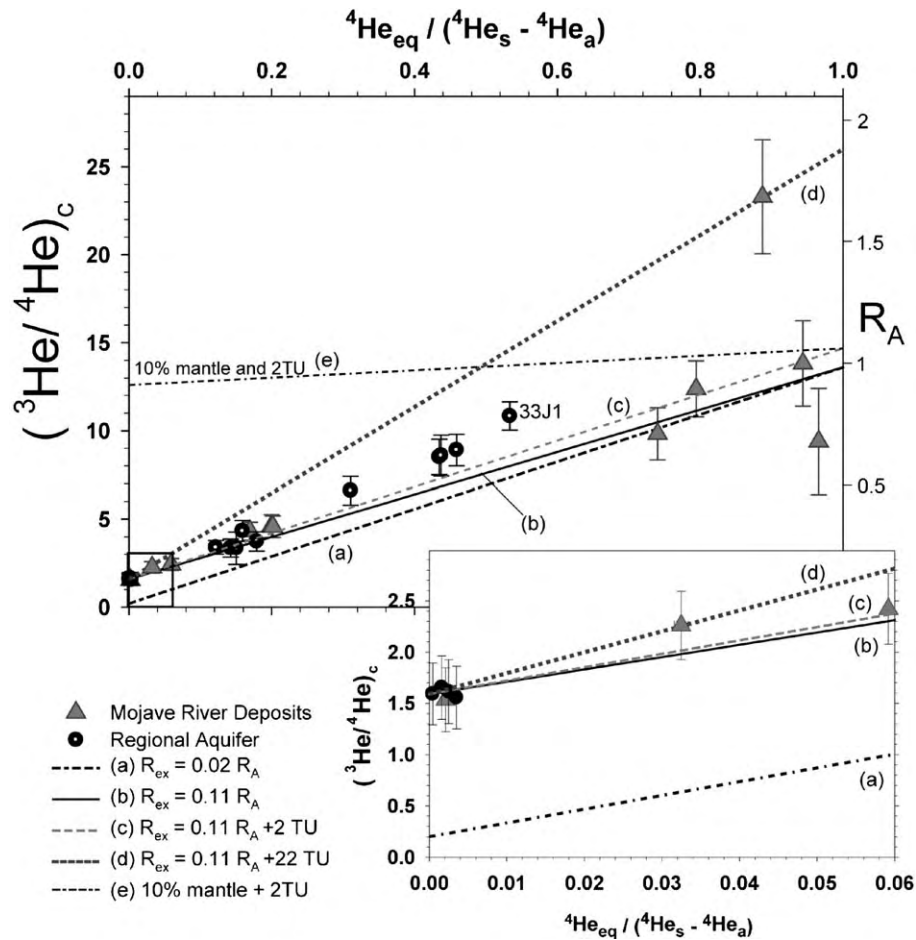


Fig. 5. Measured $^3\text{He}/^4\text{He}$ ratios corrected for air bubble entrapment versus the relative amount of ^4He owing to solubility with respect to total ^4He , corrected for air bubble entrapment. Lines (a) and (b) represent the evolution of the ratios with $^3\text{He}/^4\text{He}$ crustal ratios of 0.2×10^{-7} and 1.59×10^{-7} , respectively (see Eq. (10) in the text). No He of tritogenic origin is present in these cases. Lines (c) and (d) show the evolution of line (b) when 2 TU and 22 TU are added and totally decayed to produce 0.5 and $5.5 \times 10^{-14} \text{ cm}^3 \text{ STP g}^{-1} \text{ TU}^{-1}$ of ^3He . Line (e) represents an addition of 10% of He of mantle origin with $^3\text{He}/^4\text{He} = 1.2 \times 10^{-5}$ and taking into account an average crustal production $^3\text{He}/^4\text{He}$ ratio of 0.2×10^{-7} as well as a background ^3H content of 2 TU.

nucleogenic ^3He from lithium decay in crustal materials and/or preferential release of nucleogenic ^3He , and/or (iii) a contribution of a mantle-derived helium flux.

In the case for tritogenic ^3He , it is significant that the sample (well 4N/4W-1C4) with the highest measured $^3\text{He}/^4\text{He}$ ratio ($1.24R_A$) plots along line (d)—consistent with a starting composition equivalent to the complete decay of 22 TU superimposed on air-equilibrated water (R_{eq}) followed by addition of radiogenic helium with $R_{\text{ex}} = 1.59 \times 10^{-7}$. This site has a significant tritium signal ($^3\text{H}_{1C4} = 12.2 \text{ TU}$, see Table 1),

suggesting mixing with a large component of recent water. Precipitation in Santa Maria, CA ($\sim 300 \text{ km}$ west of the MRB), reached 700 TU during the peak of the nuclear weapons testing in 1963 (Michel, 1989); therefore, it is not surprising that some modern samples have measurable tritium contents. Other samples from the MRD have low TU and therefore a smaller contribution from modern recharge: this can explain their only slightly elevated helium isotope ratios (i.e. their position on trajectory (c) in Fig. 5). However, owing to the antiquity of most groundwater samples

(Table 1)—particularly for the regional aquifer system—and their distribution along the meteoric water line (Fig. 3), mixing with young tritium-rich water can be discounted in nearly all cases.

In order for radiogenic processes (in situ) to produce $^3\text{He}/^4\text{He}$ ratios $\sim 0.11R_A$ from the $^6\text{Li}(n, \alpha)^3\text{H} \rightarrow ^3\text{He}$ reaction, the lithium content in the aquifer material would have to be greater than 300 ppm (with the observed [U] and [Th]). Typical Li concentrations in sandstone lithologies, such as the MRB, are ~ 15 ppm (Andrews, 1985), and thus the contribution of ^3He from lithium decay may be discounted owing to the requirement of unrealistically large concentrations of lithium. However, preferential release of nucleogenic ^3He over in-situ produced ^4He may lead to $^3\text{He}/^4\text{He}$ ratios higher in the fluid phase in comparison with the production site. In the case of the MRB ($R_{\text{ex}}=0.11R_A$ vs. $R_{\text{is}}=0.02R_A$), there is a factor of ~ 6 between the fluid and the production $^3\text{He}/^4\text{He}$ ratios. In theory, therefore, complete release of ^3He and partial release ($\sim 16\%$) of ^4He could account for the ‘excess’ helium isotope ratios observed in the fluids. Although different $^3\text{He}/^4\text{He}$ ratios have been observed between fluids and rocks previously (e.g. the Carnmenellis granite–groundwater system; Martel et al., 1990) if large fractionations of ^3He and ^4He have occurred in the MRB, then groundwater ages based upon ^4He would be significantly younger compared to other chronometers. As shown in the next section, there is good agreement between ^4He and ^{14}C groundwater ages, particularly for younger waters in the regional aquifer system.

We conclude that a simple two-endmember mixing model between mantle ($R_m \sim 8R_A$) and crustal ($R_{\text{dc}} \sim 0.02R_A$) components can account for the high R_{ex} in these samples. Assuming the above endmember ratios, there is an average 1.2% mantle contribution to the total He inventory for a majority of the groundwaters in this study. A slightly higher mantle contribution (3–5%) is required to account for the four regional aquifer sites which plot between line (c) and line (d) in Fig. 5. These results are discussed in detail in Section 6.3.

6.2. Terrigenic ^4He —geochronological implications

The terrigenic contribution to the ^4He inventory is principally controlled by two components: in-situ pro-

duction within the aquifer and a deep crustal flux. Assuming that the deep crustal flux may be quantified (or neglected), the former component has chronological significance for the groundwater. Stute et al. (1992) propose an approach by which the different helium components may be separated, enabling either groundwater ages or crustal helium fluxes to be estimated.

The relationship between apparent (corrected) groundwater age (τ_{corr} , in years) and the deep crustal flux entering the aquifer (J_0 , in $\text{cm}^3 \text{He STP cm}^{-2} \text{year}^{-1}$) is given by the following equation (Stute et al., 1992):

$$\tau_{\text{corr}} = \frac{{}^4\text{He}_{\text{ex}}}{\left(\frac{J_0}{\phi z_0 \rho} + {}^4\text{He}_{\text{sol}}\right)} \quad (11)$$

where He_{ex} is the excess ^4He (${}^4\text{He}_{\text{is}} + {}^4\text{He}_{\text{dc}}$) in $\text{cm}^3 \text{STP g}^{-1} \text{H}_2\text{O}$, ϕ is the effective porosity of the aquifer, z_0 is the depth (m) at which this flux enters the aquifer, and ρ is the density of water ($\sim 1 \text{g cm}^{-3}$). Note that the ^4He solution or accumulation rate (${}^4\text{He}_{\text{sol}}$ in $\text{cm}^3 \text{STP g}^{-1} \text{H}_2\text{O year}^{-1}$) is given by the following equation which combines the radioelement content of the aquifer {in brackets} with its physical properties (e.g. Andrews and Lee, 1979):

$${}^4\text{He}_{\text{sol}} = \rho \times \lambda \times \{1.19 \times 10^{-13}[\text{U}] + 2.88 \times 10^{-14}[\text{Th}]\} \times \frac{(1 - \phi)}{\phi} \quad (12)$$

In this equation, [U] and [Th] are the uranium and thorium concentrations in the aquifer rock (ppm); ρ is the bulk density of the aquifer rock (g cm^{-3}), λ is the fraction of helium produced in the rock that is released into the water, assumed to be unity, and ϕ is the fractional effective porosity of the aquifer rock.

In circumstances in which there is no extraneous flux of helium into the aquifer ($J_0=0$), Eq. (11) reduces to:

$$\tau_r = \frac{{}^4\text{He}_{\text{ex}}}{{}^4\text{He}_{\text{sol}}} \quad (13)$$

Assuming that the MRB has the characteristics $\phi=20\%$, $\rho=2.83 \text{g cm}^{-3}$, [U]=2.3 ppm, [Th]=7.9 ppm (Bushnell and Morton, 1987; Izbicki et al., 2000), then the groundwater accumulation rate for ^4He in the MRB is $\sim 5.67 \times 10^{-12} \text{cm}^3 \text{STP g}^{-1}$

$\text{H}_2\text{O year}^{-1}$, which yields MRB groundwater ages ranging from 0.01 to >18 My (Eq. (13)). These ages are many orders of magnitude greater than ages determined by either modeled hydraulic properties (<40,000 year) or ^{14}C (see Table 1). Clearly, these results imply the presence of a significant deep crustal contribution of helium to the MRB.

In order to assess the inter-relationship between in-situ production of ^4He and the deep crustal flux (J_0), we plot the ^4He ages (calculated using Eq. (11)) versus

the interpreted ^{14}C ages of the regional aquifer groundwaters in Fig. 6. Note that we exclude the MRD groundwaters because surface-water infiltration along the entire length of the Mojave River leads to mixing of waters of differing ages, thus invalidating the assumptions behind the use of the helium chronology method. In the calculation of He age, we use the He solution rates of $5.67 \times 10^{-12} \text{ cm}^3 \text{ STP g}^{-1} \text{ H}_2\text{O year}^{-1}$ ($\phi=20\%$) and $1.28 \times 10^{-11} \text{ cm}^3 \text{ STP g}^{-1} \text{ H}_2\text{O year}^{-1}$ ($\phi=10\%$). The crustal He flux (J_0) is set

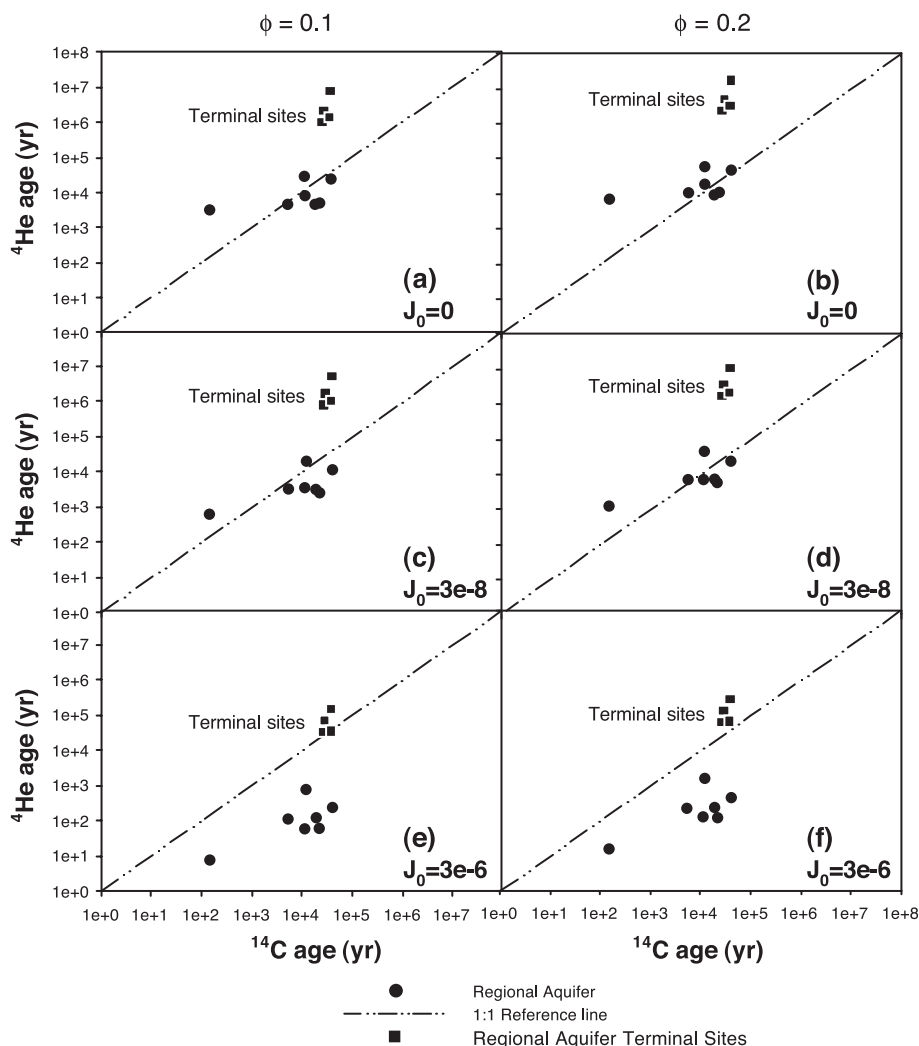


Fig. 6. Plots of ^4He groundwater ages versus interpreted ^{14}C ages taking into account three crustal fluxes ($J_0 = 0, 3 \times 10^{-8}, 3 \times 10^{-6} \text{ cm}^3 \text{ STP cm}^{-2} \text{ year}^{-1}$) with porosities $\phi = 0.1$ and 0.2 . Best agreement between ^4He and ^{14}C derived ages for recent waters are with the parameters $J_0 = 0 - 3 \times 10^{-8} \text{ cm}^3 \text{ STP cm}^{-2} \text{ year}^{-1}$, $\phi = 0.2$ (b,d), and for the terminal sites, $J_0 = 3 \times 10^{-6} \text{ cm}^3 \text{ STP cm}^{-2} \text{ year}^{-1}$, $\phi = 0.1$ (e).

at three values: zero (i.e. no crustal flux), 3×10^{-8} and 3×10^{-6} (units of cm^3 STPHe cm^{-2} year^{-1}). A J_0 value of 3×10^{-8} cm^3 STPHe cm^{-2} year^{-1} represents a low crustal flux of helium, in comparison with fluxes recorded from various aquifers worldwide (see Table 7 in Ballentine et al., 2002), whereas 3×10^{-6} cm^3 STPHe cm^{-2} year^{-1} is a 'typical' flux, characteristic of the continental crust (Ballentine et al., 2002; O'Nions and Oxburgh, 1983). In Fig. 6, the regional aquifer data cluster in two distinct age groups, older terminal groundwaters (5N/5W-4A1, 6N/4W-30N8, 4N/4W-3A2, 4N/4W-1C2) and younger samples.

We note two main points for the MRB groundwaters using the above combination of He solution rate and J_0 values: (1) the 'non terminal' regional aquifer samples (with one exception [sample 4N/7W-33J1]) show concordant ages with ^{14}C (within a factor of 2) for low-to-negligible J_0 -values (0 and 3×10^{-8} cm^3 STPHe cm^{-2} year^{-1}) in (Fig. 6b,d), and (2) the four terminal regional aquifer waters (sampled at a down-dip distance ≥ 22 km; Fig 4) require a significantly larger crustal He flux ($\geq 3 \times 10^{-6}$ cm^3 STPHe cm^{-2} year^{-1}) to approximate the ^{14}C ages.

The above calculations assume a constant He solution rate for the entire MRB: this is unlikely as the alluvial fan deposits grade from coarse grain sizes near the mountain front (recharge area) to fine grain sizes near the Mojave River (discharge area) leading to a decrease in aquifer porosity (Izbicki et al., 2000) and groundwater velocity (Stamos et al., 2001) down-dip (>22 km). However, when the He solution rate is adjusted to 1.28×10^{-11} cm^3 STP g^{-1} H_2O year^{-1} (for $\phi = 10\%$), the terminal sites (down-dip) in the regional aquifer exhibit better concordance between ^4He and ^{14}C ages (for $J_0 = 3 \times 10^{-6}$ cm^3 STPHe cm^{-2} year^{-1} ; see Fig. 6e).

The fact that the helium ages of the youngest samples exhibit closer agreement with ^{14}C ages when little or no crustal flux is present supports findings by other workers that relatively young groundwaters are dominated by in-situ He production. For example, Torgersen and Clarke (1985) found concordance between ^4He and ^{14}C ages for groundwaters up to 50 ky in the Australian Great Artesian Basin: this was explained by wells being sufficiently shallow to be above the influence of any crustal flux. This may well be the case for that part of the MRB regional aquifer close to (i.e. within ~ 22 km of) the mountain front

recharge area. Greater porosity and higher groundwater velocities near the mountain front, may result in groundwater flow that entrains little or no basal-crustal flux (see below), thereby effectively limiting the influence of the J_0 term in younger MRB groundwaters.

This is not the case down-dip in the regional aquifer (>22 km from recharge) where a crustal helium flux ($J_0 \geq 3 \times 10^{-6}$ cm^3 STPHe cm^{-2} year^{-1}) is necessary for agreement between ^4He and ^{14}C ages (Fig. 6e). A large crustal flux down-dip in the MRB is not surprising in light of (a) high He concentrations in the deeper sections of other aquifers, e.g. the Great Artesian Basin, Australia (Torgersen and Clarke, 1985) and the Paris Basin (Castro et al., 1998a,b), and (b) numerical models of groundwater flow (e.g. Bethke et al., 1999), which predict vertical structure in the distribution of aquifer helium owing to a basal flux of crustal helium in addition to horizontal 'plug-piston' flow (Zhao et al., 1998). It is noteworthy in this respect that helium concentrations in MRB groundwaters increase with depth, as observed at three multi-level monitoring well sites (see Table 1 and Fig. 2).

Introduction of the crustal flux (J_0) may occur by diffusion from underlying basement followed by entrainment and upward migration, particularly in the discharge region (Bethke et al., 2000). In this way, more basal-flux helium is entrained with increasing distance along flowpaths, and helium concentrations would be expected to increase sharply. This model fits the He observations for the MRB regional aquifer with water near the recharge area dominated by atmospheric and in-situ produced He whereas the crustal flux overwhelms these components in waters located more than 22 km down-dip.

The magnitude of J_0 needed for agreement between the helium and ^{14}C ages for the terminal groundwaters in the regional aquifer is of particular interest. Although these sites have similar lithologies, flow history, and flow distance (~ 32 km), the northern flowpath terminal sites requires a crustal flux three times larger than the nearby southern flowpath terminal sites. For the two samples from the terminus of the southern flowpath (A-B'), a crustal flux of $J_0 = 3 \times 10^{-6}$ cm^3 STPHe cm^{-2} year^{-1} produces close agreement between the two

chronometers (± 8 –19%); however, this J_0 value gives high ^4He ages (67,000 and 145,000 years) for the two samples from the terminus of the northern flowpath (A – A') (see Fig. 1). Here, we suspect that the Shadow Mountain Adelanto Fault (SMAF) gives rise to an even greater crustal helium flux. A crustal-flux value of $J_0 = 1 \times 10^{-5} \text{ cm}^3 \text{ STPHe cm}^{-2} \text{ year}^{-1}$ is necessary for agreement (± 12 –28%) between ^{14}C and helium ages of the groundwaters. The northern J_0 value is more than three times the flux identified in the southern cross-section although the sites are separated by only ~ 14 km. This observation suggests that faults may act to focus deep crustal fluids into the shallow crust, since large heterogeneities in crustal fluxes are not expected over such small distances.

The general conclusion that emerges from these observations is that application of ^4He chronology to groundwater systems needs to be undertaken on a case-by-case basis in tectonically active regions. In the case of the MRB, the in-situ ^4He accumulation method (without correction) is appropriate for groundwaters (up to 22 km from recharge) even though this section of the aquifer is unconfined. For terminal sites located downdip of ~ 22 km, the residence time of groundwaters may also be calculated given reasonable estimates of the magnitude of the crustal He flux.

6.3. Excess ^3He : tectonic implications

Resolution of the measured He contents into component structures allows identification of a mantle-derived ^3He ($^3\text{He}_m$) contribution to all samples in the MRB (waters from both the regional aquifer and the MRD). Other studies in the region close to the San Andreas Fault (SAF) which have utilized hot springs, oil and gas wells in addition to groundwaters have also observed high helium isotope ratios (up to $\sim 4R_A$, or a 50% mantle contribution) (Kennedy et al., 1997). With the close proximity of the MRB (0–33 km) to the SAF system, it is not surprising that samples in this study also contain significant concentrations of mantle-derived ^3He —given that its presence has been associated with regions undergoing active extension (Oxburgh et al., 1986; Torgersen, 1993). Assuming a binary mantle–crust mixture and end-member compositions defined previously (Section

6.1), the greatest percentage contribution of $^3\text{He}_m$ to the regional aquifer system is well 4N/7W-33J1 (5.6%). This well is situated within 0.5 km of the SAF (Fig. 1), and its relatively young groundwater is isolated from the crustal flux. It is no surprise, therefore, that this locality is sensitive to record a mantle input of He. However, the nature of the mantle input requires further examination. Is the mantle flux highly localized, with fault systems acting as conduits to the surface? Alternatively, given that fact that all wells exhibit some $^3\text{He}_m$ addition, the possibility exists that a diffuse $^3\text{He}_m$ flux pervasively invades the entire MRB.

To consider the nature of the mantle ^3He input to the MRB, we plot the absolute concentration of mantle-derived ^3He ($^3\text{He}_m$) in all samples versus distance from the SAF (Fig. 7). There are two points to note. First, the regional aquifer samples (from wells within ~ 22 km of recharge) have a fairly constant concentration of $^3\text{He}_m$ (2 – $6 \times 10^{-14} \text{ cm}^3 \text{ STP g}^{-1} \text{ H}_2\text{O}$). Second, the four terminal sites in the regional aquifer contain varying amounts of $^3\text{He}_m$, between one and three orders of magnitude more than the younger samples—the highest value being $1.5 \times 10^{-11} \text{ cm}^3 \text{ STP g}^{-1} \text{ H}_2\text{O}$. Note that with the exception of one sample (6N/4W-30N7, which contains a mix of modern and old helium-rich waters), samples from the MRD have mantle ^3He contents similar to the regional aquifer samples within 22 km of recharge. Therefore, the MRB groundwaters fall into two distinct populations—samples with relatively modest amounts of $^3\text{He}_m$, and terminal samples (located >22 km from recharge) with significantly higher $^3\text{He}_m$ contents.

This pattern or distribution of $^3\text{He}_m$ in MRB groundwaters is significant because it argues against an all-pervasive, spatially uniform $^3\text{He}_m$ flux entrained in groundwaters throughout the basin. In such a scenario, one would anticipate a gradual increase in $^3\text{He}_m$ with increasing residence time (i.e. downdip distance) of the groundwater. Such a distribution is not observed (see Fig. 7): rather, samples from sites less than 22 km from recharge exhibit fairly uniform $^3\text{He}_m$ concentrations (2 – $6 \times 10^{-14} \text{ cm}^3 \text{ STP } (^3\text{He}) \text{ g}^{-1} \text{ H}_2\text{O}$), while the terminal sites contain several orders of magnitude more $^3\text{He}_m$. To account for the high $^3\text{He}_m$ in the terminal sites, either the rate of accumulation would have to be much higher (in the

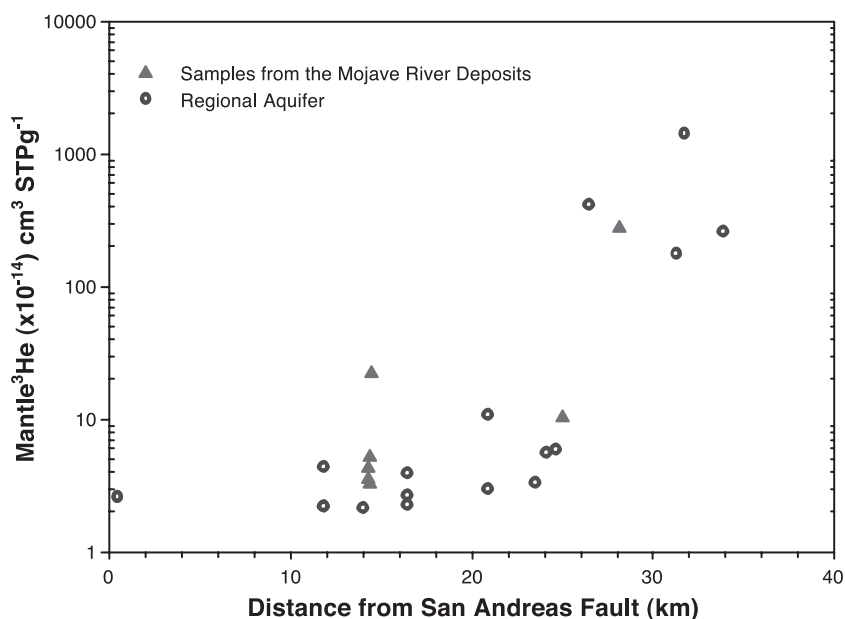


Fig. 7. Absolute concentration of mantle-derived ³He measured in groundwater samples (cm³ STPg⁻¹) as a function of the distance from the San Andreas Fault.

past) than for the more-recently recharged waters, or there is an additional source of ³He_m affecting the terminal sites only. Significantly, the groundwater ages of the terminal site waters are approximately similar to other waters (e.g. 5N/6W-22E(1–2) and 5N/7W-24D3), which do not show large ³He_m accumulations. Therefore, it is unlikely that the basin-wide accumulation rate of ³He_m has varied significantly over the past ~ 30,000 year.

We conclude that there are two discrete sources of mantle ³He in the MRB: (1) the SAF system, which contributes mantle ³He to groundwater as it recharges near the mountain front providing the ‘basin-wide’ mean ³He_m concentration of ~ 3 × 10⁻¹⁴ cm³ STPg⁻¹ H₂O, and (2) the SMAF and AVF faults which lie along and near the terminus of the groundwater flow system that introduce additional fault-related ³He_m to the groundwaters in their immediate proximity. The distribution of ³He_m in Fig. 7 is consistent with the notion that a ³He_m flux exists for wells located near faults, as opposed to being related to groundwater age. The observed changes in mantle-helium concentrations may therefore represent a tracer for either proximity to fault systems or, more speculatively, to fault activity. There is evidence that

changes in ³He/⁴He ratios are associated with earthquake activity (Ballentine and Burnard, 2002; Hilton, 1996; Sano et al., 1986; Sorey et al., 1993) although little is known regarding changes in absolute mantle fluxes. Conversely, it may be argued that the observation of a relatively constant mantle ³He concentration observed throughout the basin over the past ~ 30,000 years indicates that this section of the SAF has remained at a constant level of activity over this period. Further helium studies in a heavily faulted groundwater basin are necessary to distinguish between these explanations.

7. Concluding remarks

Groundwaters from the Mojave River Basin have a number of sources contributing to their total helium inventory. These components may be isolated using standard modeling techniques, and reasonable assumptions of endmember compositions ($R_{dc} = R_{is} = 0.02R_A$, $R_m = 8 R_A$). In addition to atmosphere-derived helium, all samples (from both the regional aquifer and MRD) have mantle-derived ³He and in-situ produced radiogenic helium; however, several of the older samples

also possess an extraneous radiogenic helium component consistent with a whole-crustal flux.

In conclusion, we emphasize the following main points from this study:

(1) Radiogenic He in all samples of the MRB allows estimates of the groundwater 'age' distribution in the basin. For the most part, there is good concordance between ^4He ages and ^{14}C ages for groundwaters in the regional aquifer (<22 km from recharge), thereby demonstrating the applicability of the ^4He -method in the present case. Terminal waters (>22 km from recharge) give significantly higher ^4He -ages in comparison with estimates based upon hydraulic properties. This observation is consistent with the presence of a whole-crustal flux of He in the MRB ($J_0 = 3 - 10 \times 10^{-6} \text{ cm}^3 \text{ STP cm}^{-2} \text{ year}^{-1}$) comparable with estimates derived for other regions worldwide. At locations where groundwater interacts with active fault systems, identified by high absolute concentrations of mantle-derived ^3He , an enhanced crustal flux is also observed suggesting a relationship between elevated mantle and crustal helium fluxes. In spite of the crustal flux, reasonable estimates of groundwater ages are still possible for the older waters once the whole crustal-flux component is resolved from the in situ produced helium.

(2) A mantle-derived helium component is observed in all samples of the MRB. This is not surprising given the basin's proximity to the SAF system. What is significant, however, is the finding that the distribution of the mantle component is associated with the location of fault systems, suggesting that faults may act as discrete conduits of mantle helium to the groundwater system. The large variation in $^3\text{He}_m$ in the terminal MRB waters may be related to proximity of active faulting or to variations in past fault activity. In the case of the second scenario, it is conceivable that groundwater may act as an archive of past seismic activity. The relative constant $^3\text{He}_m$ in MRB groundwaters younger than $\sim 30,000$ year may indicate that activity along this segment of the SAF system appears to have been relatively constant over this period.

Acknowledgements

This work was supported by the Hydrologic Sciences Program of the National Science Foundation

(award EAR-0001133) and by the United States Geological Survey Water Resources Division (San Diego). Chris Ballentine and two anonymous reviewers provided constructive remarks on the manuscript. [LW]

References

- Andrews, J.N., 1985. The isotopic composition of radiogenic helium and its use to study groundwater movement in confined aquifers. *Chem. Geol.* 49, 339–351.
- Andrews, J.N., Lee, D.J., 1979. Inert gases in groundwater from the Bunter Sandstone of England as indicators of age and paleoclimatic trends. *J. Hydrol.* 41, 233–252.
- Ballentine, C.J., Burnard, P., 2002. Production of noble gases in the continental crust. *Rev. Mineral. Geochem.* 47, 481–538.
- Ballentine, C.J., Burgess, R., Marty, B., 2002. Tracing fluid origin, transport and interaction in the crust. *Rev. Mineral. Geochem.* 47, 539–614.
- Bethke, C.M., Zhao, X., Torgersen, T., 1999. Groundwater flow and the ^4He distribution in the Great Artesian Basin of Australia. *J. Geophys. Res.* 104, 12999–13011.
- Bethke, C.M., Torgersen, T., Park, J., 2000. The "age" of very old groundwater: insights from reactive transport models. *J. Geochem. Exploration* 69–70, 1–4.
- Bushnell, M.M., Morton, P.K., 1987. Uranium favorability of the 1 degree by 2 degree Trona Quadrangle, Mojave Desert, CA. 151, CA Dept. of Conservation Division of Mines and Geology, Sacramento.
- California Department of Water Resources, 1967. Mojave River ground water basin investigation. *Bull. Calif. Dept. Water Res.* 84.
- Castro, M.C., Jambon, A., Marsily, G. de., Schlosser, P., 1998a. Noble gases as natural tracers of water circulation in the Paris Basin. 1. Measurements and discussion of their origin and mechanisms of vertical transport in the basin. *Water Resour. Res.* 34 (10) 2443–2466.
- Castro, M.C., Gobleb, P., Ledoux, E., Violette, S., Marsily, G de., 1998b. Noble gases as natural tracers of water circulation in the Paris Basin. 2. Calibration of a ground water flow model using noble gas isotope data. *Water Resour. Res.* 34 (10) 2467–2483.
- Castro, M.C., Stute, M., Schlosser, P., 2000. Comparison of ^4He ages and ^{14}C ages in simple aquifer systems: implications for groundwater flow and chronologies. *Appl. Geochem.* 15, 1137–1167.
- Craig, H., Lupton, J.E., 1981. Helium-3 and mantle volatiles in the ocean and oceanic crust. In: Emiliani, C. (Ed.), *The Sea*. Wiley, New York, pp. 391–428.
- Davis, S.N., Bentley, H.W., 1982. Dating groundwater, a short review. In: Currie, L.A. (Ed.), *Nuclear and Chemical Dating Techniques: Interpreting the Environmental Record*. Amer. Chem. Soc. Symp. Ser., vol. 176, pp. 187–222.
- Davis, S., DeWiest, R.J., 1966. *Hydrogeology*. Wiley, New York. 463 pp.

- Friedman, I., Smith, G.I., Gleason, J.D., Warden, A., Harris, J.M., 1992. Stable isotope composition of waters in Southeastern California. 1. Modern precipitation. *J. Geophys. Res.-Atmos.* 97, 5795–5812.
- Hilton, D.R., 1996. The helium and carbon isotope systematics of a continental geothermal system—results from monitoring studies at Long Valley caldera (California, USA). *Chem. Geol.* 127, 269–295.
- Izbicki, J.A., in preparation. Source, movement, and age of ground water in the western part of the Mojave Desert, Southern California, USA: Part 1, delta oxygen-18 and delta deuterium data.
- Izbicki, J.A. and Michel, R.L., in preparation. Source, movement, and age of ground water in the western part of the Mojave Desert, Southern California, USA: Part 2, Tritium and carbon-14 data.
- Izbicki, J.A., Martin, P., Michel, R.L., 1995. Source, movement and age of groundwater in the upper part of the Mojave River Basin, California, USA. In: Adair, E.M., Leibungut, C. (Eds.), *Application of Tracers in Arid Zone Hydrology*. IAHS Publ., Vienna, pp. 43–56.
- Izbicki, J.A., Michel, R.L., Martin, P., 1998. Chloride and tritium concentrations in a thick unsaturated zone underlying an intermittent stream in the Mojave Desert, southern California, USA. In: Brahana, J. (Ed.), *Gambling with Groundwater—Physical, Chemical, and Biological Aspects of Aquifer-Stream Relations*. Am. Inst. Hydrol. St. Paul, MN, pp. 81–88.
- Izbicki, J.A., Radyk, J., Michel, R.L., 2000. Water movement through a thick unsaturated zone underlying an intermittent stream in the western Mojave Desert, southern California, USA. *J. Hydrol.* 238, 194–217.
- Kennedy, B.M., Kharaka, Y.K., Evans, W.C., Ellwood, A., DePaolo, D.J., Thordsen, J., Ambats, G., Mariner, R.H., 1997. Mantle fluids in the San Andreas fault system, California. *Science* 278, 1278–1281.
- Kipfer, R., Aeschbach-Hertig, W., Peeters, F., Stute, M., 2002. Noble gases in lakes and ground waters. *Rev. Mineral. Geochim.* 47, 615–700.
- Kulongoski, J.T., Hilton, D.R., 2002. A quadrupole-based mass spectrometric system for the determination of noble gas abundances in fluids. *Geochem. Geophys. Geosyst.* 3, U1–U10.
- Kulongoski, J.T., Hilton, D.R., Izbicki, J.A., in preparation. Noble gas studies in Mojave Desert, California: Climate implications.
- Lines, G.C., 1996. Ground-Water and surface-water relations along the Mojave River, Southern California. 95-4189, USGS, Sacramento, California.
- Mamyrin, B.A., Tolstikhin, I.N., 1984. Helium Isotopes in Nature. Elsevier, Amsterdam. 273 pp.
- Martel, D.J., O’Nions, R.K., Hilton, D.R., Oxburgh, E.R., 1990. The role of element distribution in production and release of radiogenic helium—the Cammenellis granite, southwest England. *Chem. Geol.* 88, 207–221.
- Michel, R.L., 1989. Tritium deposition in the continental United States, 1953–83. 89-4072, U.S. Geol. Surv., Reston, Virginia.
- O’Nions, R.K., Oxburgh, E.R., 1983. Heat and helium in the earth. *Nature* 306, 429–431.
- Oxburgh, E.R., O’Nions, R.K., Hill, R.I., 1986. Helium isotopes in sedimentary basins. *Nature* 324, 632–635.
- Ozima, M., Podosek, F.A., 1983. *Noble Gas Geochemistry*. Cambridge; New York: Cambridge University Press, p. 267.
- Plummer, L.N., Preteomon, E.C., Parkhurst, D.L., 1994. An interactive code (NETPATH) for modeling NET geochemical reactions along a flow PATH-Version 2.0. U.S. Geol. Surv. Water Res. Invest. Rep., 94–4169.
- Sano, Y., Nakamura, Y., Wakita, H., Notsu, K., Kobayashi, Y., 1986. $^3\text{He}/^4\text{He}$ ratio anomalies associated with the 1984 Western Nagano earthquake: possibly induced by a diapiric magma. *J. Geophys. Res.* 91, 12291–12295.
- Smith, G.I., Friedman, I., Gleason, J.D., Warden, A., 1992. Stable isotope composition of waters in southeastern California 2. Groundwaters and their relation to modern precipitation. *J. Geophys. Res.-Atmos.* 97, 5813–5823.
- Sorey, M.L., Kennedy, B.M., Evans, W.C., Farrar, C.D., Suemnicht, G.A., 1993. Helium isotope and gas discharge variations associated with crustal unrest in Long Valley Caldera, California, 1989–1992. *J. Geophys. Res.-Solid Earth* 98, 15871–15889.
- Stamos, C.L., Martin, P., Nishikawa, T., Cox, B.F., 2001. Simulation of ground-water flow in the Mojave River Basin, CA. U.S. Geol. Surv., Rep. 01-4002, Sacramento, California.
- Stute, M., Sonntag, C., Deak, J., Schlosser, P., 1992. Helium in deep circulating groundwater in the Great Hungarian plain—flow dynamics and crustal and mantle helium fluxes. *Geochim. Cosmochim. Acta* 56, 2051–2067.
- Subsurface Surveys, 1990. Inventory of Groundwater Stored in the Mojave River Basins. Subsurface Surveys, Solana Beach, CA, p. 47.
- Torgersen, T., 1980. Controls on pore-fluid concentrations of ^4He and ^{222}Rn and the calculation of $^4\text{He}/^{222}\text{Rn}$ ages. *J. Geochem. Explor.* 13, 57–75.
- Torgersen, T., 1993. Defining the role of magmatism in extensional tectonics: He^{-3} fluxes in extensional basins. *J. Geophys. Res.* 98, 16257–16269.
- Torgersen, T., Clarke, W., 1985. Helium accumulation in groundwater: I. An evaluation of sources and continental flux of crustal ^4He in the Great Artesian basin, Australia. *Geochim. Cosmochim. Acta* 49, 1211–1218.
- Weise, S., Moser, H., 1987. Groundwater Dating with Helium Isotopes. IAEA, Vienna.
- Weiss, R.F., 1971. Solubility of helium and neon in water and seawater. *J. Chem. Eng. Data* 16, 235–241.
- Zhao, X., Fritzel, T.L.B., Quinodoz, H.A.M., Bethke, C.M., Torgersen, T., 1998. Controls on the distribution and isotopic composition of helium in deep ground-water flows. *Geology* 26, 291–294.